



Experimental investigation on the cooling performance of polystyrene encapsulated n-Docosane based nanofluid in mini channel heat sink

Mathew Joseph^{1,2} · E V Jitheesh³ · V Sajith¹

Received: 26 August 2020 / Accepted: 29 March 2021 / Published online: 11 April 2021
© The Author(s), under exclusive licence to Springer-Verlag GmbH Germany, part of Springer Nature 2021

Abstract

The present work focusses on the comparative study of cooling performance of nano encapsulated phase change material (nanoPCM) based heat transfer fluid (PCM nanofluid) and deionized water in a minichannel heat sink (MCHS) with a hydraulic diameter of 2.6 mm. Polystyrene encapsulated n-Docosane was synthesised by mini emulsion polymerisation. The melting point and latent heat of nanoPCM was found to be 42.6 °C and 180.6 J/g respectively. PCM nanofluid with concentrations ranging from 0.6 to 1.5 vol.% was prepared by dispersing nanoPCM in deionized water. High zeta potential values indicated excellent suspension stability of PCM nanofluid. Viscosity of PCM nanofluid increased slightly, whereas thermal conductivity and density were comparable to deionized water. Experiments were conducted at different flow rates (75–450 mL/min) in the laminar flow regime under uniform heat flux of 2.6 W/cm². Even though, PCM nanofluid at 0.7 vol.% showed an enhancement in heat transfer up to 44% at 225 mL/min, as compared to water, pumping power increased up to 17%. However, the Figure of Merit values greater than unity shows the insignificance of increase in pumping power over heat transfer enhancement obtained for PCM nanofluid. The improved cooling performance at low flow rates makes PCM nanofluid a propitious coolant over conventional fluids for electronics cooling.

Keywords Heat transfer enhancement · Minichannel heat sink · Nanoencapsulated PCM · nanoPCM · PCM nanofluid

Nomenclature

\bar{h}	Average heat transfer coefficient (W/m ² K)
\bar{Nu}	Average Nusselt number
Q	Heat energy (W)
A	Area (m ²)
T	Temperature (K)
k	Thermal conductivity (W/m K)
q_{flux}	Heat flux (W/m ²)
c_p	Specific heat (kJ/kg K)
\dot{m}	Mass flow rate (kg/s)
P	Power (W)
V	Voltage (V)

I	Current (A)
Q_{loss}	Heat loss (W)
p	Pressure (Pa)
D_h	Hydraulic diameter (m)
u	Flow velocity (m/s)
z	Vertical distance (m)
L	Characteristic length (m)
n	Number of channels (m)
P_m	Pumping power (W)
R	Thermal resistance (K/W)

Greek symbols

ρ	Density (kg/m ³)
μ	Dynamic viscosity (Pa.s)

Dimensionless groups

Nu	Nusselt number
Re	Reynolds number
Pr	Prandtl number

Subscripts

f	Fluid
-----	-------

✉ V Sajith
sajith@nitc.ac.in

¹ School of Materials Science and Engineering, National Institute of Technology Calicut, Kozhikode, Kerala, India

² Department of Mechanical Engineering, Rajagiri School of Engineering and Technology, Cochin, Kerala, India

³ Department of Mechanical Engineering, National Institute of Technology Calicut, Kozhikode, Kerala, India

<i>in</i>	Inlet
<i>out</i>	Outlet
<i>w</i>	Wall
<i>cond</i>	Conduction
<i>conv</i>	Convection
<i>nf</i>	Nanofluid
<i>bf</i>	base fluid
<i>ch</i>	Channel
<i>w</i>	Width
<i>h</i>	Height
<i>abs</i>	Absorbed

Acronyms

PCM	Phase change material
PCMNF	Phase change material based nanofluid
DI	Deionized
TEM	Transmission electron microscope
PSA	Particle size analyser
FT-IR	Fourier transform infrared
DSC	Differential scanning calorimetry
FOM	Figure of merit
MCHS	Minichannel heat sink

1 Introduction

Electronics thermal management using solid-liquid phase change materials (PCMs) has gained significant practical interest in the past decade. High latent heat of fusion, reduced space requirements owing to high energy density per unit volume, and wide range of phase change temperature makes PCM a suitable candidate for electronics cooling. However, PCM based passive cooling techniques are found to be inadequate for many applications like cooling of high heat flux power electronics including IGBTs, military and medical equipment, desktop microprocessors, lasers etc. In such cases, liquid based cooling is an effective method for controlling the temperature of electronic devices. In liquid cooling systems, a liquid coolant is circulated through micro/minichannel heat sinks using mechanical pumps for the heat dissipation. Kandilkar and Grande [1] classified the channels based on their hydraulic diameter (D_h) into conventional channels ($D_h > 3\text{mm}$), minichannels ($200\ \mu\text{m} < D_h < 3\ \text{mm}$), micro channels ($10\ \mu\text{m} < D_h \leq 200\ \mu\text{m}$). Even though micro channel heat sinks offer high heat transfer coefficient the pressure drop is quite high [2, 3]. Liquid coolant based minichannel heat sink (MCHS) experience less pressure drop as compared to micro channel heat sinks [4, 5]. However, the main issue with minichannel based liquid cooling systems is the lower heat transfer capability of the coolants.

Many works on the use of nanomaterials for enhancement of heat transfer capability of coolants in MCHSs has been reported. Thermal conductivity enhanced nanofluids are synthesized by

dispersing metal, metal oxide or carbon based nanoparticles in base fluids. However, the poor stability of nanofluid causes settlement of nanoparticles, leading to clogging of channels and reduced heat transfer [6, 7]. The increased viscosity of these nanofluids leads to larger pressure drop and pumping power [8, 9].

Charunyakorn et.al [10], Goel et.al [11], Yamagishi et.al [12], and Han et.al. [13] theoretically demonstrated that effective heat capacity of the fluid can be increased by dispersing PCM in base fluid. Accordingly, the effective heat capacity of PCM based heat transfer fluid is given by, $C_{eff} = C_o + \frac{\phi H_{PCM}}{\Delta T}$, where C_o is the heat capacity of base fluid, ϕ and H_{PCM} are the volume fraction and latent heat of dispersed PCM respectively, and ΔT is the difference between fluid temperature and melting temperature of dispersed PCM. Recently, heat capacity enhanced fluids were synthesised by dispersing micro or nanoencapsulated PCMs in water [14–16]. The encapsulated PCMs consists of a core-shell structure in which PCM is wrapped in a polymer shell. The encapsulated PCMs are usually spherical in shape. The PCM encapsulation permits solidification of PCM without leakage while maintaining the suspension stability and heat transfer efficiency of PCM. The thermal performance of encapsulated PCM based fluids is governed by size and geometry of encapsulation as well as the shell material and its thickness [17–20]. The encapsulated PCMs are divided into two main categories according to the size of particle. The encapsulated PCM with particle size ranging from 1 to 1000 nm is referred to as nanoencapsulated PCM (nanoPCM), whereas the size of microencapsulated PCM (microPCM) is from 1 to 1000 μm [21].

Rao et.al [22] experimentally investigated the water-based microPCM suspension of PMMA encapsulated n-octadecane with different mass concentrations ranging from 0 to 20%, in a rectangular MCHS of 2.71 mm hydraulic diameter. Dammal et.al [23] used PMMA encapsulated n-eicosane microPCM suspension in 9 parallel copper minichannels, each 50 mm long with a cross-sectional area of 2 mm \times 4.2 mm. The average wall temperature was found to be decreased considerably with microPCM suspension as compared to water for all heat fluxes in the range 0.4794 W/cm² to 1.9176 W/cm². Ho et.al [24] compared the thermal performance of microPCM suspension in MCHS having a hydraulic diameter of 1.2 mm with that of water. The maximum heat transfer effectiveness for microPCM suspension was 52% for $Re = 133$. Ho et.al [25] compared the cooling performance of water based suspensions of alumina and microencapsulated n-eicosane in a MCHS (dimensions 1 mm \times 1.5 mm \times 50 mm). Alumina nanofluid showed better heat transfer performance as compared to alumina and microPCM hybrid suspension. To conclude, for microPCM suspensions, there exist a certain parameter combination at which the latent heat effect dominates, resulting in heat transfer enhancement. Also, the residence time of micro PCM particles in the channel should be long

enough for the phase change to occur. The cooling performance increased at low flow rates and deteriorated at higher concentration of microPCM. The heat transfer effectiveness was found to be improved with reduction in sensible to latent heat ratio of microPCM suspension [21]. Due to high particle concentration and larger size of microPCM particles, the micro encapsulated PCM suspensions have poor suspension stability resulting in the separation under the influence of gravity. In addition, high fluid viscosity results in crushing of large particles during pumping, especially at high volume fractions and hence microPCM suspensions are not reliable for repeated thermal cycles. In addition, the viscosity, pressure drop and pumping power increases drastically with concentration of microencapsulated PCM [26–28].

The nanoPCM based fluids is a propitious solution to overcome the above disadvantages. The traditional synthesis methods of microPCM are not suitable for nanoPCM due to the smaller size of particles [17]. Miniemulsion polymerisation is the most common method for the synthesis of nanoPCM and is capable of encapsulating alkane PCM with polystyrene or PMMA shell, possessing high stability [29]. Miniemulsion polymerisation was used by Fuensanta et.al [30] and Zhang et.al [31] for the synthesis of nanoPCM with average particle size less than 200 nm. Fang et.al. [32, 33] synthesised polystyrene encapsulated n-tetradecane and n-octadecane of particle size 132 nm and 124 nm respectively, using miniemulsion polymerisation. Miniemulsion polymerisation was employed to synthesize PMMA encapsulated n-dodecanol by Chen et.al [34]. Fang et.al. [35] synthesised polystyrene encapsulated n-dotriacontane by miniemulsion polymerisation. The encapsulation of the PCM results in slight alteration of their properties. After encapsulation, the latent heat dropped from 285 J/g for bulk PCM to 174.8 J/g for nanoPCM and melting point decreased from 71.1 °C to 70.9 °C. Felix De Castro et.al [36] obtained polyurethane encapsulated n-Docosane by miniemulsion polymerisation. The difference in crystallinity of polyurethane shell and PCM core due to spatial confinement and encapsulation resulted in reduction of phase transition temperature and enthalpy for encapsulated docosane. As compared to microPCM, nanoPCM has got many advantages like smaller size and hence larger specific surface area. NanoPCMs are also structurally more stable and the fracture rate is less as compared to microPCMs. In addition, due to close contact of nanoPCM and heat transfer fluid, the resistance to heat transfer is less in nanoPCM suspensions [37].

Few authors have investigated the application of nanoPCM based fluids for thermal management of electronics. Wu et al. [38] reported that with 28 vol.% of nanoPCM slurry, the heat transfer performance of jet impingement and spray cooling enhanced by 50% and 70% respectively. Wu et al. [39] investigated pressure drop and heat transfer characteristics of silica encapsulated Indium nanoPCM slurry (9 and 30 wt.%) in

micro channel heat exchanger. The heat transfer enhancement is mainly due to improved heat capacity of nanoPCM and the increase in pressure drop with nanoPCM slurry is less compared to bare PCM slurry. Seyf et al. [40] reported that nanoPCM slurry in micro channel heat sink lowers the entropy generation and wall temperature, even though the increase in mass concentration of slurry increase the pressure drop. Ho et.al [41] investigated urea-formaldehyde encapsulated n-eicosane based nanoPCM emulsion in tapered MCHS. The heat transfer was reported to be enhanced up to 10% corresponding to a heat flux of 3.21 W/cm² for 2 wt.% of nanoPCM emulsion, but the viscosity of nanoPCM emulsion was found to be very high which increased the pumping power significantly. Mathew and Sajith [42] investigated the cooling performance of polystyrene encapsulated n-octadecane based nanofluid in a 8 mm square channel and reported heat transfer enhancement up to 37% at 200 mL/min. Kuravi et.al [43] studied 100 nm sized nanoPCM in microchannel heat sink and reported large pressure drop with increase in mass concentration of slurry. Rajabifar [44] reported that nanoPCM based coolants can boost the cooling performance in micro channels. It was also reported that the wall temperature and pumping power was found to be minimum for an optimum concentration of 0.2 vol.%.

Most of the authors concluded that in the case of micro channel heat sinks, the fluid viscosity and pumping power considerably increases especially at higher concentrations of nanoPCM. Accordingly, the minichannel heat sinks are more appropriate for the use of nanoPCM based fluids. In addition, the potential for heat transfer enhancement and thermal energy storage capacity of nanoPCM based fluid can be achieved only if the temperature of base fluid is in the phase transition range of PCM. Hence it has become imperative to use nanoPCM based fluids in minichannel heat sinks at an optimum flow rate and concentration, ensuring that the nanoPCM particles are in the melting range and the phase change occurs during its circulation with in the minichannel itself.

In the previous work by the authors [42], the effect of mass flow rate and heat flux on heat transfer and pressure drop characteristics of polystyrene encapsulated n-octadecane based PCM nanofluid was studied in a single square conventional channel test section of 8 mm hydraulic diameter. Even though few works were reported on the use of nanoPCM in micro channels, the cooling performance of a stable concentration of polystyrene encapsulated n-docosane based heat transfer fluid in minichannel heat sink has not been investigated. The present work focusses on the application of polystyrene encapsulated n-docosane based PCM nanofluid in a minichannel heat sink (MCHS) with 13 channels (hydraulic diameter 2.6 mm), in the context of electronics cooling. Polystyrene encapsulated n-Docosane (nanoPCM) was synthesised by miniemulsion polymerisation and dispersed in DI water to obtain the PCM nanofluid (PCMNF). The cooling

performance of PCM nanofluid was investigated for different flow rates. The important thermo-physical properties were determined and stability studies of PCMNF was conducted. The effect of Reynolds number and flow rate of PCMNF on the heat transfer coefficient, Nusselt number, heat transfer effectiveness, average wall temperature, thermal resistance, and figure of merit (FOM) were studied in this work.

2 Materials and methods

2.1 NanoPCM synthesis

The phase change material used in the present work was n-Docosane ($C_{22}H_{46}$, Sigma Aldrich) and the monomer used was Styrene (Sigma Aldrich). AIBN solution (α - α' Azoisobutyronitrile, Sigma Aldrich) was the initiator to generate free radical for polymerisation reaction. Triton™ X-100 (Sigma Aldrich) and Oleylamine (Sigma Aldrich) were the water-soluble surfactant and oil-phase stabilizer respectively.

The synthesis of polystyrene encapsulated n-Docosane (nanoPCM) was done using miniemulsion polymerisation

technique. The detailed synthesis procedure and preparation of PCMNF is given in the previous work [42]. The mechanism of the miniemulsion polymerisation reaction is shown in Fig. 1.

2.2 Characterisation

2.2.1 Differential scanning calorimetry and FT-IR spectroscopy

The phase change characteristics of bulk PCM and nanoPCM were determined using DSC (DSCQ20, TA instruments). To ensure accuracy and repeatability of measurements, two samples of nanoPCM synthesized separately were tested. In the DSC test, the samples were heated and cooled between 0 °C and 90 °C at a rate of 5 °C/min. In order to obtain the heat capacity, three different runs were conducted in DSC. Initially, the samples were cooled down from room temperature to 0 °C and maintained at 0 °C for 5 min. The sample was then heated to 90 °C at a ramp rate of 5 °C/min and maintained at 90 °C for 5 min. The cycle was completed by cooling the sample from 90 to 0 °C at the same rate. The nanoPCM was

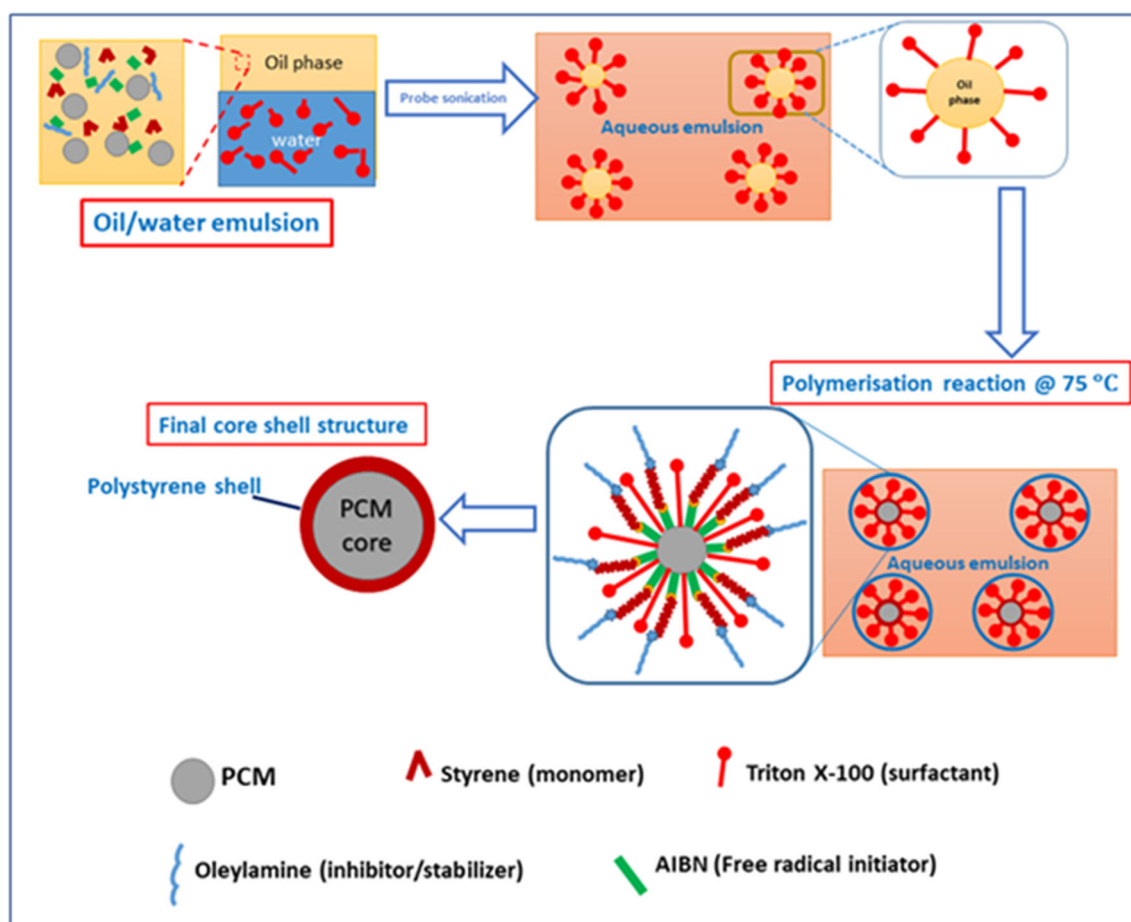


Fig. 1 Mechanism of miniemulsion polymerisation process

analysed for the formation of polystyrene shell using Fourier Transform Infrared spectroscopy (ThermoFisher Scientific). From the IR spectrum the chemical structure and bond formation in bulk and nanoPCM were analysed.

2.2.2 Particle size and suspension stability

The average size of nanoPCM and suspension stability of the nanofluid based on the Zeta potential (ZP) were determined using Particle Size Analyser (Nano-ZS, Malvern™). Different concentrations of PCMNF, 0.6 to 1.5 vol.%, was used for the stability study. For the estimation of particle size, two different samples of PCMNF was prepared and each sample was tested thrice in the Particle size analyser.

2.2.3 Thermal and mechanical stability

The thermo-cycling tests and thermo gravimetric analysis (TGA) measurements were done to confirm thermal stability of nanoPCM. For thermo-cycling tests, certain quantity of nanoPCM was heated and cooled above and below its melting point for 200 cycles repeatedly. The phase change characteristics of this PCM was then analysed in DSC after 50 cycles and 200 cycles. The TGA of bulk and nanoPCM was performed in a thermal analysis system (Q50, TA instruments). The samples were heated in nitrogen atmosphere from 26 °C to 650 °C in a platinum pan at a rate of 10 °C/min and the loss in weights were estimated. The TEM (JEOL 2100) images of nanoPCM in

PCMNF, before and after pumping experiments in MCHS were taken to study the shell rupture and mechanical stability.

2.2.4 Thermo-physical properties

Experiments were conducted to estimate the thermo-physical properties of PCMNF. Various concentrations of nanofluid in the range 0.5 to 1.5 vol.% were tested. To ensure repeatability of measurements, three samples of each concentration were synthesised and two trials were performed for each sample concentration.

The density was estimated at ambient conditions for four different concentrations (0.5, 0.7, 1 and 1.5 vol.%) of PCMNF and DI water using Pycnometer (Kyoto Electronics KEM™ - DA-130 N). KD2 Pro thermal analyzer was used to measure the thermal conductivity of PCMNF (0.5, 0.7 and 1.5 vol.%) and DI water. The viscosity was measured for different concentrations of PCMNF (0.5, 0.7, 1 and 1.5 vol.%) and DI water in the temperature range 30 to 80 °C using Rheometer (MCR 102, Anton Paar).

2.3 Experimental setup

The schematic of the experimental setup is shown in Fig. 2. The experimental setup consists of the minichannel heat sink integrated with a heater and flow circuit with control. The schematic representation of minichannel array and layout of the minichannel is shown in Fig. 3(a) and (b) respectively. The

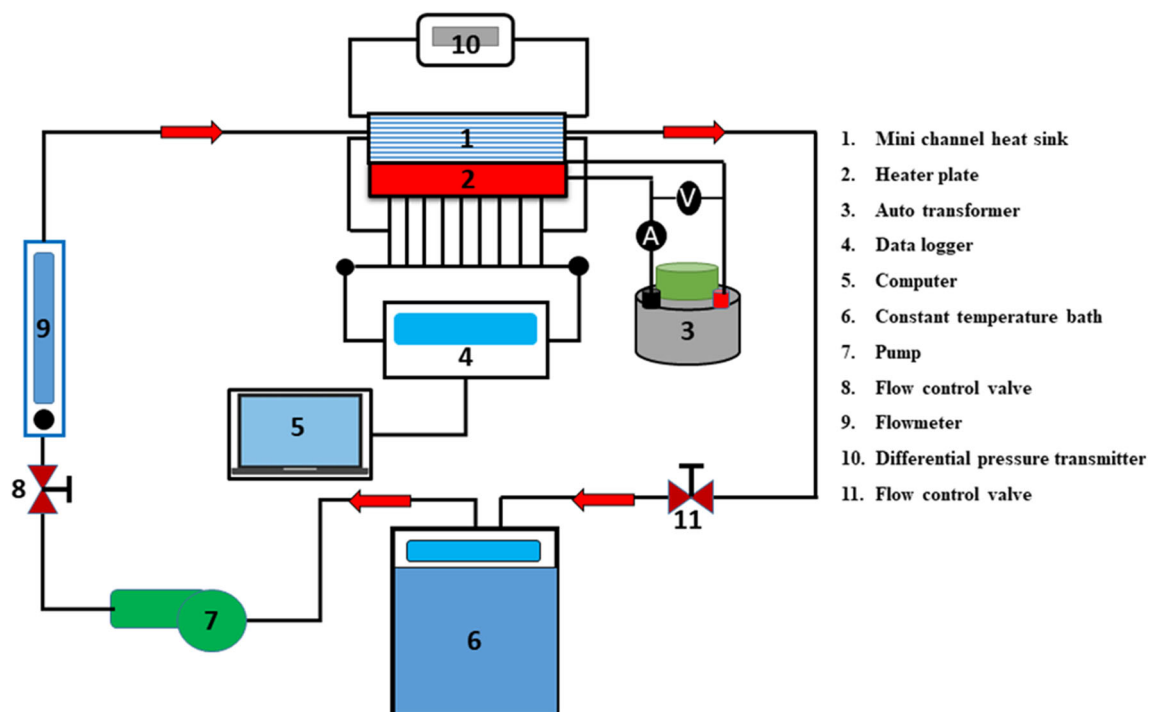
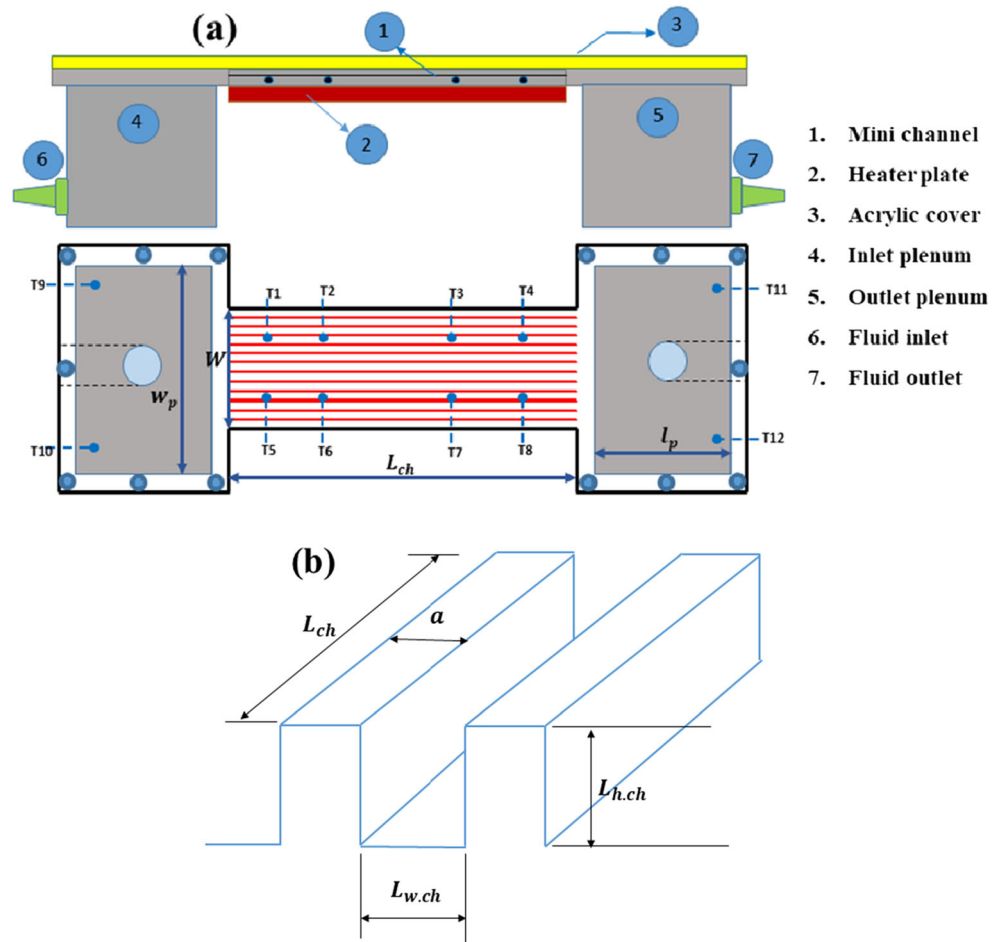


Fig. 2 Schematic of experimental set up

Fig. 3 a Schematic of minichannel array b Layout of the minichannel



dimensions of the minichannel are given in Table 1. MCHS consists of 13 straight channels having uniform cross sectional area and hydraulic diameter of 2.64 mm and was made from aluminium by CNC milling. The minichannels are connected by inlet and outlet plenums to establish uniform flow through channels. The entire minichannels and the plenums were covered by transparent acrylic sheet aiding flow visualization and also for thermal insulation. A plate heater (106 mm × 61 mm ×

3 mm) was thermally pasted beneath the MCHS to simulate the generation of heat flux from microprocessors. The plate heater was fabricated by winding nichrome wire coils over a thin sheet of mica. The input power to the plate heater was adjusted by an auto-transformer. The side and bottom walls of the MCHS and heater assembly was thermally insulated using glass wool and wood to minimize the heat losses.

The test fluid is filled in a small reservoir and placed in constant temperature bath. The test fluid was circulated through the MCHS using a submersible pump and the heat absorbed by the fluid in the minichannels was rejected in the temperature bath, thus maintaining a constant inlet temperature for the test fluid.

The flow rate was measured using a flow meter and was controlled by a needle valve attached to it. To measure temperature at various locations in the MCHS, T-type thermocouples were calibrated and connected to data acquisition system (Agilent, 34972A, LXI). The thermocouple locations are shown in Fig.3(a). Eight equally spaced T-type thermocouples placed centrally along the channel width and 1.5 mm below the minichannel wall surface, were used for measuring the local base temperature along heat sink length. The fluid inlet

Table 1 Dimensions of the minichannel heat sink

Parameter	Symbol	Dimension (mm)
Minichannel length	L_{ch}	106.4
Minichannel width	$L_{w.ch}$	2.2
Minichannel height	$L_{h.ch}$	2.6
Minichannel fin spacing	a	2.6
Minichannel array width	W	61.4
Minichannel plenum length	l_p	32.2
Minichannel plenum width	w_p	80.4
No. of channels	n	13

and outlet temperatures were measured by four T-type thermocouples placed at the inlet and outlet plenums. The pressure drop incurred during the flow was measured by a pressure transmitter (Yokogawa, Japan) fitted between the inlet and outlet sections of the MCHS.

3 Theory

The hydraulic diameter of the MCHS [24] is,

$$D_h = \frac{L_{w.ch}L_{h.ch}}{2(L_{w.ch} + L_{h.ch})} \quad (1)$$

The mass flow rate of fluid through MCHS,

$$\dot{m} = \dot{Q}_f \rho_f \quad (2)$$

where, \dot{Q}_f is the volume flow rate of fluid.

The heat flux due to conduction through the MCHS is given by,

$$q_{flux} = \frac{P}{A_{cond}} \quad (3)$$

The power dissipated by plate heater is,

$$P = VI \cos \phi \quad (4)$$

$\cos \phi$ is the power factor (≈ 0.9).

The heat gained by the working fluid is given as,

$$Q_{abs} = \dot{m} c_p (T_{out.f} - T_{in.f}) \quad (5)$$

The percentage heat loss [3] is estimated as,

$$Q_{loss} = \left(\frac{P - Q_{abs}}{P} \right) \times 100 \quad (6)$$

The mean difference between the power supplied and the energy absorbed by the moving fluid, was found to be less than 10%, which indicates that heat loss that occurs from the test module to the surroundings is negligible.

The average heat transfer coefficient [3],

$$\bar{h} = \frac{Q_{abs}}{A_{conv}(T_{w.avg} - T_{mean})} \quad (7)$$

The convection heat transfer area [24] is,

$$A_{conv} = n(2L_{h.ch} + L_{w.ch})L_{ch} \quad (8)$$

The bulk mean temperature of fluid is,

$$T_{mean} = \frac{T_{in.f} + T_{out.f}}{2} \quad (9)$$

The averaged wall temperature of MCHS [3] is given as,

$$T_{w.avg} = \frac{1}{8} \sum_{i=1}^8 \left(T_{w,i} - \frac{s q_{flux}}{k_{Al}} \right) \quad (10)$$

where, $T_{w,i}$ is the base temperature shown by individual thermocouple, s is the distance between MCHS bottom surface and position of thermocouples (1 mm), k_{Al} is the aluminium thermal conductivity (205 W/mK), q_{flux} is the flux due to heat conduction.

The average Nusselt number [24] is estimated from the following equation,

$$\overline{Nu} = \frac{\bar{h} D_h}{k_f} \quad (11)$$

The flow Reynolds number [25] is estimated as,

$$Re = \frac{\dot{m} D_h}{\mu n A_c} \quad (12)$$

where, $A_c = \frac{\pi}{4} D_h^2$, is the channel cross sectional area of a single minichannel and n is the number of channels in the MCHS.

The skin friction coefficient [5] is defined as,

$$f = \frac{D_h \Delta p}{2 L_{ch} \rho_f u^2} \quad (13)$$

The pressure drop can be measured from the differential pressure transmitter connected across the MCHS,

$$\Delta p = p_{in} - p_{out} \quad (14)$$

The bulk fluid velocity [24] is calculated as,

$$u = \frac{\dot{Q}_f}{n A_c} \quad (15)$$

The pumping power [24] is given as,

$$P_m = \frac{\dot{m} \Delta p}{\rho_f} \quad (16)$$

The average and maximum thermal resistance of MCHS [25] is given by,

$$R_{avg} = \frac{T_{w.avg} - T_{in.f}}{Q_{abs}} \quad (17)$$

$$R_{max} = \frac{T_{w.max} - T_{in.f}}{Q_{abs}} \quad (18)$$

where, $T_{w.max}$ is the maximum wall temperature of MCHS.

The percentage heat transfer enhancement [5] is given as,

$$\text{Heat transfer enhancement} = \frac{\overline{Nu_{nf}} - \overline{Nu_{bf}}}{\overline{Nu_{bf}}} \times 100 \text{ (\%)} \quad (19)$$

Figure of merit combines both the effects of heat transfer improvement and pumping power penalty [25]. It is defined as,

$$FOM = \frac{\left(\frac{\overline{h_{nf}}}{\overline{h_{bf}}} \right)}{\left(\frac{P_{m,nf}}{P_{m,bf}} \right)^{1/3}} \quad (20)$$

4 Uncertainty analysis

The estimation of primary data using instruments and calculation of physical parameters brings errors and hence it is necessary to quantify these errors. The instruments were calibrated to obtain the uncertainties in primary measurements. The thermocouples were calibrated using standard procedure and the uncertainty in temperature measurements were obtained. The uncertainty in the derived quantities were obtained by Taylor's theorem [45]. The maximum uncertainty associated with the input parameters and measured parameters is shown in Table 2. The maximum absolute uncertainty for heat

transfer coefficient and pumping power measurement were found to be within $\pm 4\%$. The maximum uncertainties in measurement of output parameters in the experiments were estimated to be less than $\pm 7\%$ which indicates the reliability of the measured data.

5 Result and discussion

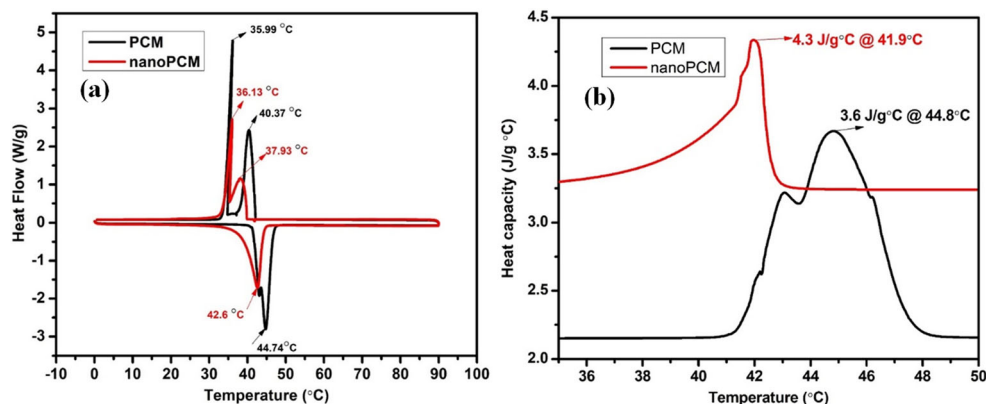
5.1 Differential scanning calorimetry and FT-IR spectroscopy

The phase change characteristics and the heat capacity variation of bulk PCM and nanoPCM are shown in Fig.4(a) and (b) respectively. The peak areas on the DSC curve represents the melting/ solidification enthalpies, and the apex temperatures of the respective peaks were taken as the melting/ solidification temperatures. From the DSC curves, the peak temperature and latent heat during melting of bulk PCM (n-Docosane) were found to be $44.75 \text{ }^\circ\text{C}$ and 237 J/g respectively. Similarly, the peak solidification temperature and enthalpy were estimated as $40.37 \text{ }^\circ\text{C}$ and 229 J/g respectively. The melting point and latent heat of fusion for nanoPCM was obtained as $42.6 \text{ }^\circ\text{C}$ and 180.7 J/g respectively. The peak solidification temperature and enthalpy of nanoPCM were

Table 2 Uncertainty analysis

Parameter (units)	Symbol	Range	uncertainty
Input parameters			
Voltage (V)	V	100–200	± 0.01
Current (A)	I	0.5–1.2	± 0.01
Hydraulic diameter of channel (mm)	D_h	0–2.7	± 0.0001
Length (mm)	L_{ch}	0–50	± 0.0001
Measured parameters			
Mean fluid temperature ($^\circ\text{C}$)	$T_{f, \text{mean}}$	36.6–56.5	± 0.25
Avg. wall temperature ($^\circ\text{C}$)	$T_{\text{wall, avg}}$	41.8–70.0	± 0.25
Pressure drop (mm of H_2O)	Δp	52.9–176.5	± 0.065
Flow rate (mL/min)	vol_f	50–500	$\pm 2\%$
Output parameters			
Power (W)	P	50–180	$\pm 2.5\%$
Heat absorbed by fluid (W)	Q_{abs}	149.5–152.4	$\pm 3.5\%$
Avg. heat transfer coefficient ($\text{W/m}^2\text{K}$)	\overline{h}	1097.6–2485.3	$\pm 3.7\%$
Avg. Nusselt number	\overline{Nu}	4.39–10.79	$\pm 4.0\%$
Pumping power (W)	P_{pumping}	$6.61 \times 10^{-5} - 1.32 \times 10^{-3}$	$\pm 3.2\%$
Reynolds number	Re	50–350	$\pm 2.6\%$
Friction factor	f	0.297–3.68	$\pm 2.0\%$
Avg. thermal resistance (K/W)	$R_{th, \text{avg}}$	0.054–0.182	$\pm 4.8\%$
Enhancement factor	EF	0.254–0.444	$\pm 6.5\%$
Figure of merit	FOM	1.14–1.29	$\pm 6.2\%$

Fig. 4 a Phase change characteristics of bulk and nanoPCM b Specific heat capacity variation of bulk and nanoPCM



37.93 °C and 175 J/g respectively. The melting point was found to be dropped by 2 °C and latent heat was found to be decreased by 23% for nanoPCM, in comparison to bulk PCM. The mechanism of decrease in latent heat, shift in melting peak and increase in specific heat of nanoPCM is explained in previous work by authors [42].

The FTIR spectrum of n-Docosane and polystyrene encapsulated n-Docosane is shown in Fig.5. From the FTIR spectrum of n-Docosane, the characteristics peaks at 2954 cm^{-1} , 2913 cm^{-1} , 2872 cm^{-1} and 2848 cm^{-1} represents the C-H bond stretching vibration in $-\text{CH}_2$ and $-\text{CH}_3$ groups. The characteristic peak corresponding to 1471 cm^{-1} , 1454 cm^{-1} and 1370 cm^{-1} confirms the asymmetric bending of $-\text{CH}_2$ and $-\text{CH}_3$ groups. The peak at 717 cm^{-1} represents the rocking vibration of $-\text{CH}_2$ groups. In case of nanoPCM, the peak at 1576 cm^{-1} is the aromatic C=C stretching vibration absorption which confirms the existence of benzene rings in nanoPCM. The peak at 2934 cm^{-1} represents the existence of methylenes and the peak at 3318 cm^{-1} shows the stretching vibration absorption of O-H indicating the existence of hydroxyl groups.

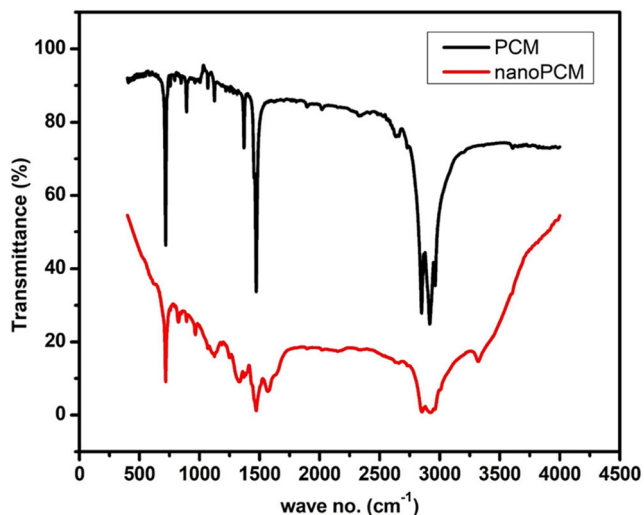


Fig. 5 FT-IR spectra of bulk PCM and nanoPCM

5.2 Particle size and suspension stability

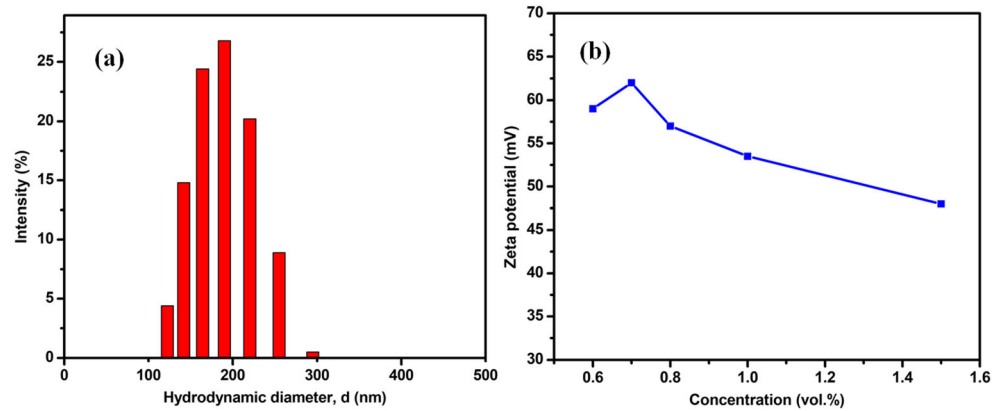
The average hydrodynamic diameter of the particles dispersed in the PCMNf was measured by means of Dynamic light scattering system. Based on the different trials, the result corresponding to minimum poly dispersion index value is shown in Fig.6(a), indicating average hydrodynamic diameter of 195 nm.

The zeta potential values of various concentrations of PCMNf is depicted in the Fig.6(b). The zeta potential gives the magnitude of electrostatic repulsion between similarly charged particles in the colloidal suspension. The highest zeta potential of 62 mV was obtained at 0.7 vol.%, and decreased thereafter. With increase in concentration, the surfactants on the nanoPCM surface interacts, leaving the nanoPCM and forms separate micelles and reduces the zeta potential. In fact, if zeta potential values lies between $\pm 30\text{ mV}$ and $\pm 50\text{ mV}$, there is chance of flocculation of the dispersion and when zeta potential values are more than $\pm 60\text{ mV}$, the dispersion will resist aggregation of particles [46]. Hence, 0.7 vol.% of PCMNf demonstrating highest suspension stability was used for experimentation in the present work.

5.3 Thermal and mechanical stability

The TGA curve of bulk and nanoPCM is shown in Fig.7(a). No significant change in decomposition temperature was visible for nanoPCM as compared to bulk PCM up to a temperature of 230 °C. Hence, it can be inferred that encapsulation of PCM will not affect the thermal stability of PCM in this temperature range. Nevertheless, it may be noted that beyond 230 °C, the weight loss of nanoPCM was reduced compared to bulk PCM, until 375 °C. This clearly indicates that in the case of nanoPCM, the polystyrene shell protects the volatile decomposition of PCM at higher temperature thus improving the thermal stability of PCM. The DSC curves of nanoPCM after 50 and 200 thermal cycles are shown in Fig.7(b). The thermo-cycling tests shows that there is no significant change in the latent heat and melting temperature of nanoPCM even

Fig. 6 **a** Hydrodynamic diameter of nanoPCM **b** Zeta potential variation for PCMNF



after 200 thermal cycles and hence it is very much suitable for continuous operation. The TEM images of nanoPCM in nanofluid prior to pumping and after pumping experiments in the MCHS are shown in Fig.8(a) and (b) respectively. It is observed that even after repeated flow through pumps and channels, the shells are not broken, ensuring high mechanical stability for nanoPCM.

5.4 Thermo-physical properties of PCMNF

5.4.1 Density

The density of DI water and PCMNF at various concentrations is shown in Fig.9(a). It is found that there is negligible change in density of DI water with addition of nanoPCM. The density of n-Docosane and for the present work is 0.794 g/cc and 1.05 g/cc respectively [36]. Therefore, as per effective medium theory, PCMNF density decreases with concentration increase. Even so, at stable concentration of 0.7 vol.%, the effective density of PCMNF is comparable with DI water.

5.4.2 Thermal conductivity

The thermal conductivity of PCMNF and DI water is given in Fig.9(b). Negligible changes in thermal conductivity of DI

water was observed after nanoPCM addition, due to the low thermal conductivity of PCM (0.23 W/mK) and the shell (0.21 W/mK). Even though the Brownian motion of nanoPCM is present in PCMNF, the low thermal conductivity of polystyrene shell resist the thermal diffusivity and heat flow, hence insignificant change in thermal conductivity was observed for PCMNF. A slight decrease in thermal conductivity of PCMNF was found with increase in the particle concentration, due to agglomeration of the particles.

5.4.3 Viscosity

The variation of viscosity of PCMNF with respect to temperature and concentration is given in Fig.9(c). The absolute viscosity of PCMNF increased at higher concentrations. In the temperature range 30 to 80 °C, the viscosity for PCMNF (0.7% v/v concentration) was found to be enhanced up to 14.5% relative to DI water. With increase in concentration, there is a strengthening of shear force between the nanoPCM particles, hindering the movement of fluid layers on each other resulting viscosity increase of nanofluid. Figure 9(c) illustrates that the increase in temperature reduces the fluid viscosity. This decrease in viscosity is mainly due to weakening of intermolecular attraction between the fluid and

Fig. 7 **a** TGA of bulk and nanoPCM **b** Therocycling stability tests for nanoPCM

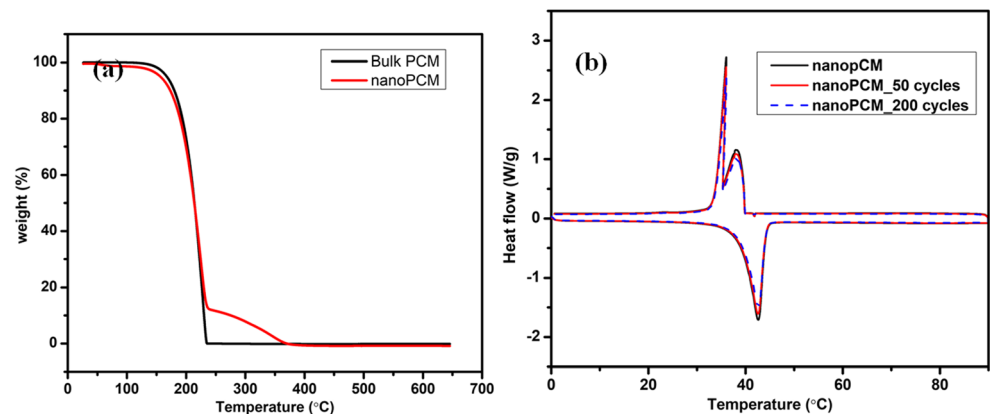
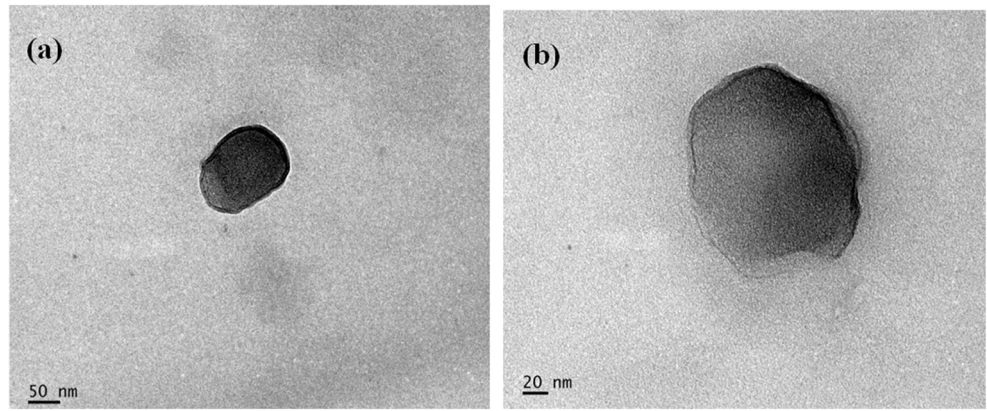


Fig. 8 TEM image of nanoPCM in PCMNF **a** before experiment **b** after experiments in MCHS



nanoparticles with rise in temperature. The encapsulation of PCM with in polystyrene shell prevents its contact with the fluid and hence no significant effect in viscosity was observed during the melting of PCM in the shell.

5.5 Heat transfer performance

This section discusses the heat transfer performance, pressure drop and pumping power characteristics of DI water and PCMNF in MCHS. Experiments in MCHS were performed

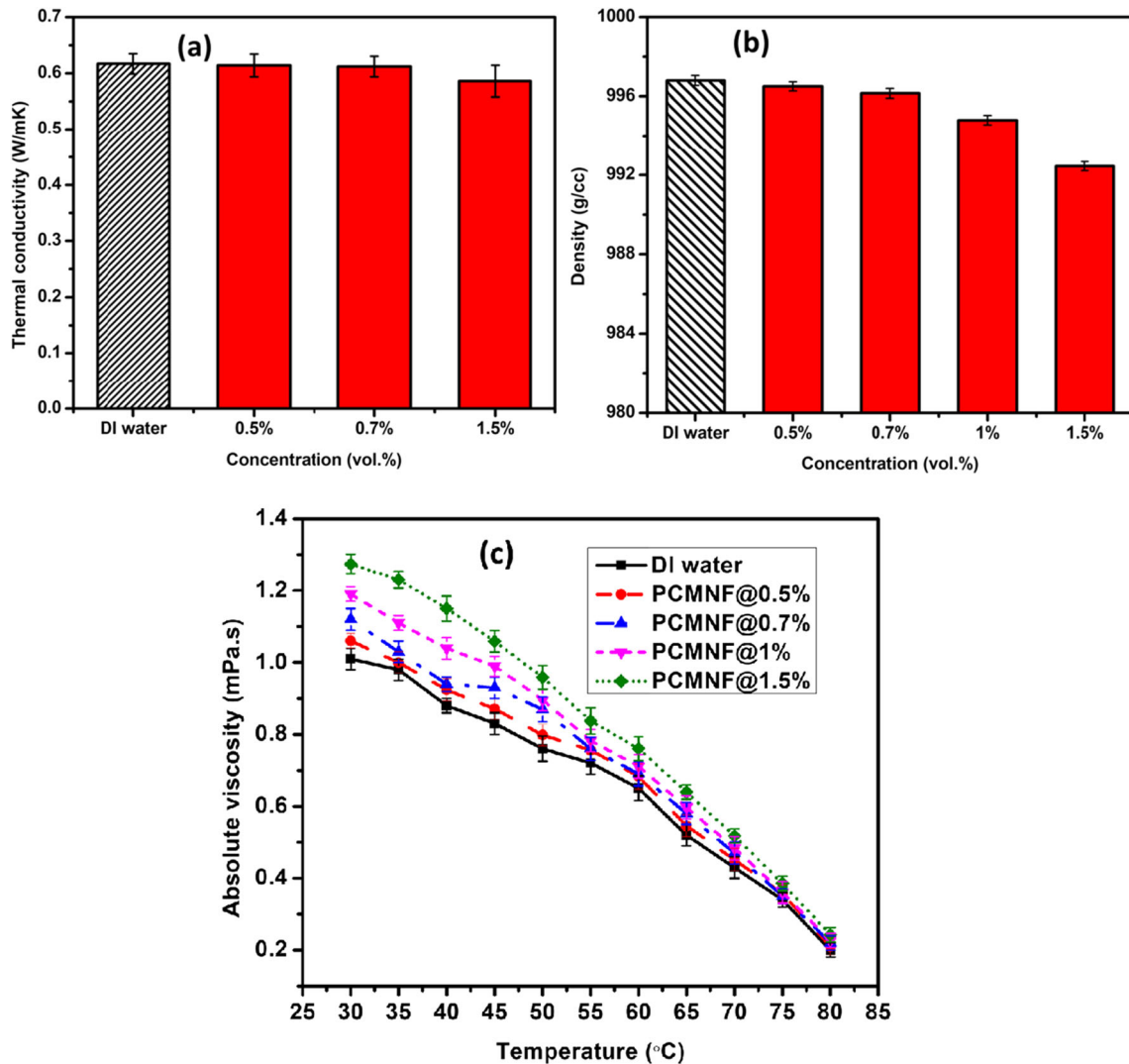


Fig. 9 Thermo-physical properties of PCMNF with concentration **a** Density **b** Thermal conductivity **c** Viscosity variation with temperature

at volume flow rates, from 75 mL/min to 450 mL/min for a constant heat flux of 2.6 W/cm². In accordance with stability studies, all experiments were conducted for nanoPCM concentration of 0.7 vol.% in DI water.

5.5.1 Experimental validation

The hydrodynamic entrance length, L_h and the thermal entrance length, L_{th} for fluid flow through MCHS [47] is given by,

$$L_h = 0.05 Re D_h \quad (21)$$

$$L_{th} = 0.1 Re Pr D_h \quad (22)$$

The length of MCHS was found to be more than L_h and L_{th} . Therefore, the flow through MCHS was divided into three regions: the thermally and hydrodynamically developing flow region, hydrodynamically developed but thermally developing flow region and the fully developed flow region.

For thermally and hydrodynamically developing flow, the Nusselt number correlation proposed by Stephan and Preußer [48] is given by,

$$Nu = 4.364 + \frac{0.086 \left(\frac{Re Pr D_h}{L} \right)^{1.33}}{1 + 0.1 Pr \left(\frac{Re D_h}{L} \right)^{0.83}} \quad (23)$$

For hydrodynamically developed and thermally developing flow, the Shah correlation [48] is given by,

$$Nu = 1.953 \left(\frac{Re Pr D_h}{L} \right)^{0.33} \quad (24)$$

For fully developed flow, the Nu correlation is given by [47],

$$Nu = 3.608 \quad (25)$$

The comparison of averaged theoretical Nu based on the above correlations with Nu of DI water based on experiments at different Re is shown in Fig. 10. Using least square method in regression analysis, a linear fit was obtained and the goodness of fit was estimated. There was less than 10% deviation between the theoretical and experimental Nu , thus validating the experimental set up.

5.5.2 Fanning friction factor

Figure 11 shows the variation of Fanning friction factor with mass flow rate of the coolants. The Fanning friction factor is calculated based on Eq. (13). It can be seen that the friction factor decreases with increase in mass flow rate of the coolants, which may be due to the reduction in viscosity at increased flow rates. As skin friction coefficient is proportional to inverse of square of velocity, increasing flow rate causes a

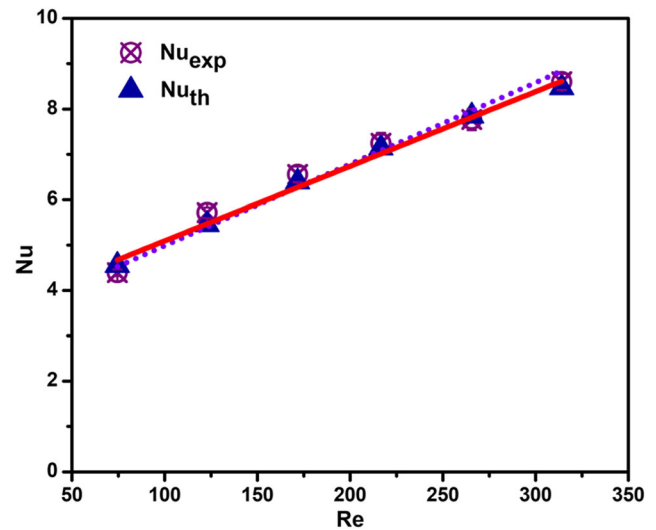


Fig. 10 Comparison of theoretical and experimentally determined Nu

decrease in skin friction coefficient. Fanning friction factor of PCMNF is seen to be slightly higher than DI water at all flow rates owing to the rise in the dynamic viscosity of PCMNF over DI water.

5.5.3 Base temperature and thermal resistance

The average wall temperature obtained with PCMNF is shown in Fig. 12. The data was fitted by a third order polynomial and the goodness of fit was determined. The wall temperature decreased with increase in mass flow rate for both the fluids, owing to an increase in heat transfer, resulting from increased turbulence. Also, for the same flow rate, the average wall temperature obtained with PCMNF is less than DI water. The drop in wall temperature for PCMNF increased with mass flow rate initially, followed by a decrease at higher flow rates.

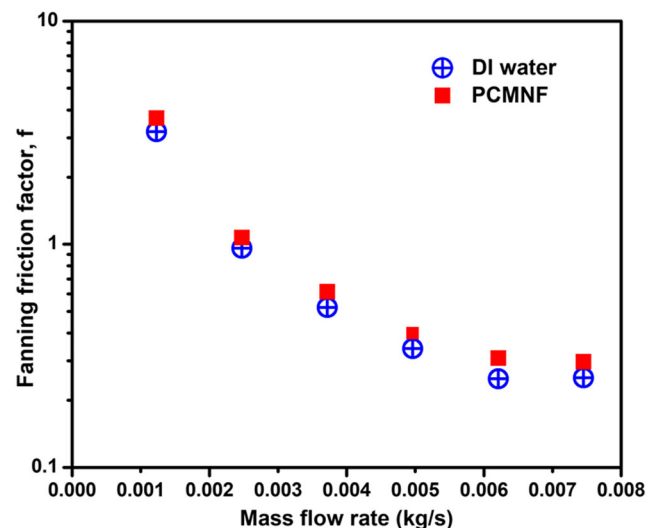


Fig. 11 Comparison of Fanning friction factor with mass flow rates

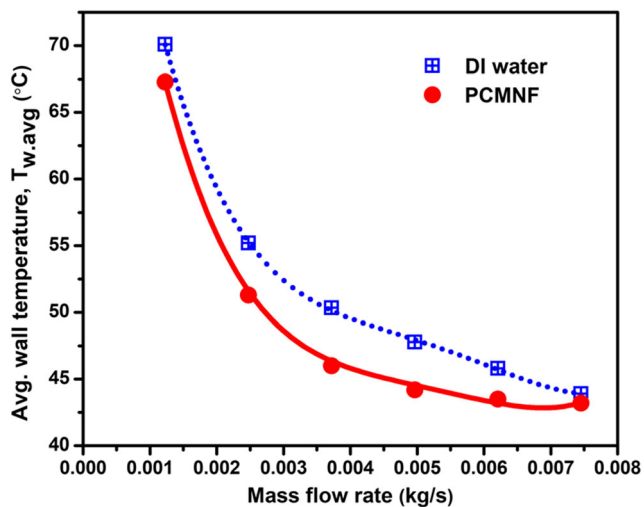


Fig. 12 Comparison of average wall temperature with mass flow rates

The average wall temperature with PCMNF lowered by up to 4.3 °C than DI water, corresponding to a mass flow rate of $3.7 \times 10^{-3} \text{ kg/s}$ (225 mL/min). Figure 12 shows that the wall temperature drop obtained with PCMNF at flow rates of $1.2 \times 10^{-3} \text{ kg/s}$ (75 mL/min) and $2.4 \times 10^{-3} \text{ kg/s}$ (150 mL/min) is slightly less than that obtained at $3.7 \times 10^{-3} \text{ kg/s}$. At low flow rates, the residence time of nanoPCM in the MCHS is high. Hence PCM will melt in a shorter distance from the inlet of MCHS, consequently the latent heat absorption by the PCM mainly occurs in that shorter distance and sensible heat absorption dominates in the remaining length of MCHS, thus reducing the heat transfer. As the flow rate increases, nanoPCM will get enough time to undergo phase change, over the entire channel length, thereby absorbing the heat from the base fluid in the form of latent heat resulting in the decrease in wall temperature. With increase in flow rate, the heat transfer increases also due to increase in turbulence resulting in the drop in wall temperature, even though it is not that much significant. However, at higher mass flow rates, as the residence time of PCM is less, phase change phenomenon will not be completed within the channel length in MCHS, thus adversely affecting the heat transfer due to latent heat absorption. The wall temperature drop was found to be reduced for PCMNF at elevated mass flow rates. Hence it is clear that for obtaining the full benefit of the PCM based fluid, the mass flow rate has to be optimized based on the resident time of nanoPCM in the MCHS depending upon the length of the flow.

The variation of average and maximum wall temperature thermal resistances with mass flow rate for PCMNF and DI water is depicted in Fig. 13. The highest value of average thermal and maximum thermal resistance was observed for DI water; whereas the lowest values were obtained for PCMNF. Since the maximum and average thermal resistances for PCMNF is lower than DI water, the addition of nanoPCM

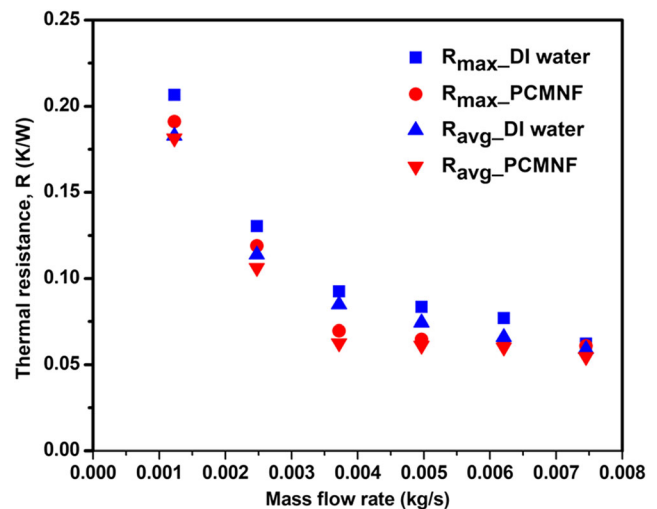


Fig. 13 Comparison of maximum and average wall thermal resistances with mass flow rates

in DI water will improve the convective heat transfer in MCHS. The results show that the wall temperature thermal resistances of both fluids varies inversely with flow rate.

MCHS may be divided into three regions according to the temperature of PCMNF. Near the entrance, the PCM is in solid phase with relatively low heat capacity. The heat transfer in this region is mainly due to the temperature difference between MCHS wall and PCMNF, and least influenced by the heat capacity of the coolant. The region where the PCM melts inside the shells and the effective heat capacity of the coolant in this region is the sum of latent heat and sensible heat. The heat transfer mechanism within this region is due to the effective heat capacity of PCMNF. Towards the end of channel, as the PCM is melts completely, only sensible heat is absorbed in this region, thereby lowering the heat capacity of the coolant leading to minimum heat transfer. The wall temperature and thermal resistance with PCMNF will be minimum along the region where both sensible and latent heat transfer are present and higher along the region with sensible heat transfer alone. From Figs. 12 and 13, at low flow rates in the range 1.2×10^{-3} to $2 \times 10^{-3} \text{ kg/s}$, the heat transfer occurs mostly in the first region where there is only sensible heat absorption and hence the reduction in wall temperature and thermal resistance for PCMNF over DI water is less. At flow rates between $2 \times 10^{-3} \text{ kg/s}$ and $7 \times 10^{-3} \text{ kg/s}$, the heat transfer occurs in the region where there is both sensible and latent heat absorption, thus providing larger drop in wall temperature and thermal resistance for PCMNF relative to DI water. Above the mass flow rate of $7.5 \times 10^{-3} \text{ kg/s}$, the heat transfer takes place mainly due to sensible heat, as the flow rate is high and PCMNF temperature is low enough to melt the PCM, hence there is no significant difference in wall temperature and thermal resistance for PCMNF over DI water. The non-uniformity in wall temperature and thermal resistance along the channel for PCMNF depends on the flow rates and residence time of

encapsulated PCM in MCHS. Melting temperature range of PCM is the critical factor affecting the temperature uniformity and thermal resistance with PCMNF with flow rates.

5.5.4 Heat transfer performance

To study the heat transfer performance of PCMNF and DI water in MCHS, the heat transfer coefficients obtained with both fluids were compared with respect to mass flow rate, as shown in Fig. 14. The heat transfer coefficient increased with mass flow rate for both fluids. Higher heat transfer coefficient than DI water was obtained for PCMNF at all flow rates. The heat absorption capacity of DI water is increased by adding nanoPCM. As the nanoPCM melts, it absorbs latent heat of fusion from the DI water and therefore, at a specific flow rate, the PCMNF absorbs more heat from the source relative to DI water. The increased heat absorption by PCMNF reduces the wall temperature in the minichannel consequently increasing the heat transfer coefficient for PCMNF over DI water. It should be noted that the heat transfer enhancement with PCMNF occurs, given that operating temperature is within the melting range of nanoPCM. The nanoPCM can absorb latent heat as long as the fluid temperature is above the melting point of PCM. Figure 14 shows that as the flow rate is increased the improvement in heat transfer coefficient for PCMNF over DI water decreases. The increase in mass flow rate reduces the residence time for melting of PCM thereby reducing the benefit obtained by the latent heat absorption in the case of PCMNF, resulting in lower heat transfer enhancement. At initial mass flow rates in the range 1.2×10^{-3} to 2×10^{-3} kg/s, the particle residence time is more and PCM melts completely at a short distance from channel entrance. In addition, at these very low flow rates, the thermal boundary layer thickness is more resulting in low heat transfer coefficient.

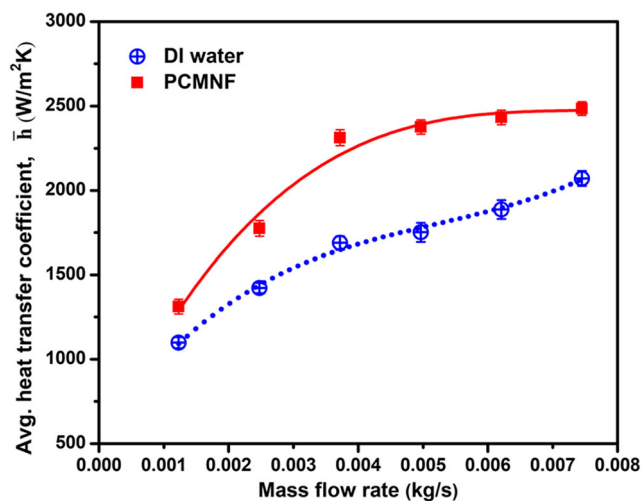


Fig. 14 Comparison of average heat transfer coefficients with mass flow rate

Increasing the flow rates further, reduces the thermal boundary layer thickness and contributes to improvement in the heat transfer coefficient for PCMNF. Figure 15 shows the variation of the average Nu with Re for both PCMNF and DI water at a heat flux of 2.6 W/cm^2 . The heat transfer and Nu increases with Re for both fluids. In the case of DI water, the heat transfer is mainly due to sensible heat gain. For PCM nanofluid, the Nu variation with Re can be divided into two regions. In region 1 ($55 < Re < 140$), there is steep increase in Nu with Re , whereas in region 2 ($140 < Re < 260$), the increase in Nu with Re is gradual. In the region 1, the enhancement in Nu is predominantly due to the latent heat absorption resulting from the melting of nanoPCM. For lower Re in the region 1, the enhancement of Nu for PCMNF with respect to DI water is found to be less than that corresponding to Re towards the end of region 1. At very low Re , the flow rate is such that the fluid temperature rise near the MCHS inlet shoot up and surpasses the melting range of nanoPCM well before the MCHS exit. Hence the latent heat absorption by the nanoPCM occurs only in a shorter length of the MCHS resulting in a decrease in Nu . Towards the end of region 1, the Re is such that the latent heat absorption is maximum as complete melting of PCM occurs entirely in the MCHS. In region 2, the heat transfer enhancement due to increased flow rate dominates the enhancement due to latent heat absorption. This is because at higher flow rates the nanoPCM may not get enough time to melt completely within the MCHS length and the latent heat effect diminishes. Therefore at higher Re , the heat transfer improvement for PCMNF is mainly due to the effect of turbulence.

Hence, it may be concluded that there is an optimum value of Re at which the improvement in heat transfer with PCMNF is maximum. The heat transfer effectiveness with PCMNF can be enhanced by properly adjusting the flow rate.

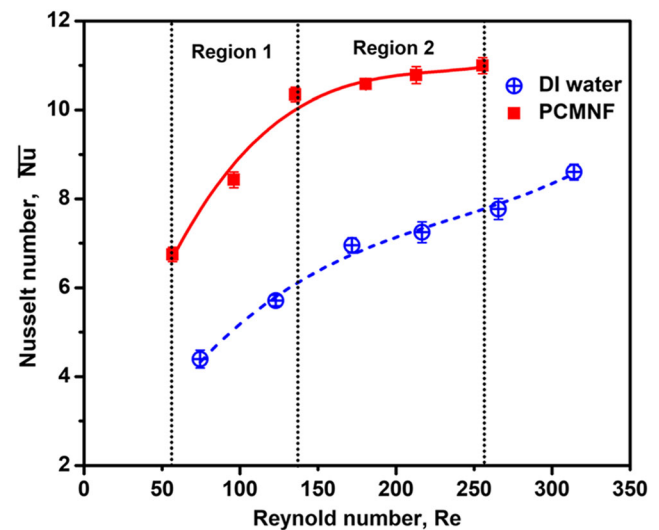


Fig. 15 Nusselt number variation with Reynolds number for PCMNF and DI water

5.5.5 Comparison of results

In this section, the present experimental findings are compared with the previous experimental data. Table 3 summarises the comparison of data for various types of PCM and its phase change properties, encapsulation, and the test section. A comparison of average Nusselt number in the present and previous works with different PCM enhanced fluids in MCHSs [22, 40, 41, 49] is shown in Fig. 16. It is clear that the average Nusselt numbers in this work are closer to that reported by Seyf et al. [40]. However, experiments in MCHS with micro encapsulated PCM based fluids [22, 41, 49] showed comparable enhancements in average Nusselt number only at higher Reynolds number. Thus, use of nano encapsulated PCM based fluids in mini channels can considerably reduce the pumping power in addition to improved heat transfer enhancement, when compared to micro encapsulated PCM based fluids. Also, the present experiments show higher average Nusselt number at low Reynolds numbers over DI water in micro channel heat sink, as reported by Lee et al. [48]. Therefore, the use of nano encapsulated PCMs improves the cooling performance in minichannel as compared to microchannels. Consequently, the use of nanoencapsulated PCM based fluid in minichannel heat sink can significantly reduce the additional pressure drop and manufacturing costs associated with microchannel heat sink, in addition to improved heat transfer.

5.5.6 Heat transfer enhancement

The percentage heat transfer enhancement shown in Fig. 17 gives the Nu enhancement with flow rates for the PCMNF. The improvement in heat transfer with PCM nanofluid over DI water is estimated based on Eq. (19). The heat transfer enhancement was found to be 29.6 and

35%, corresponding to flow rates of 75 and 150 mL/min, respectively. At low flow rates, latent heat absorption occurs mainly in the entrance section of the channel due to faster melting of PCM and only sensible heat gain occurs over the subsequent channel length, as mentioned earlier. Maximum heat transfer enhancement of 44.4% was obtained for a flow rate of 225 mL/min and the minimum heat transfer enhancement of 25.4% at 450 mL/min. The enhancement in heat transfer has been obtained due to the absorption of latent heat by the PCM during the phase change phenomena, thereby enhancing the heat capacity of the base fluid.

5.5.7 Pressure drop and pumping power

The addition of nanoPCM increases the viscosity of DI water causing pressure drop increase and pumping power rise. Figure 18 illustrates the increase in pressure drop of PCMNF and DI water against mass flow rate. With increase in mass flow rate the pressure drop was found to increase for both the fluids. Moreover, the PCMNF exhibited a marginal pressure drop rise than DI water, mainly at higher mass flow rates. This increase in pressure drop is due to the higher viscosity of PCMNF as well as the increase in the skin friction factor for PCMNF over DI water. Even though the viscosity increase was negligible at temperatures beyond 70 °C, 10 to 14.5% higher viscosity than DI water was observed for PCMNF in the temperature range 30 to 60 °C. This viscosity increase retards the liquid at the MCHS surface, increasing the stagnant liquid layer thickness at the wall surface and hence increases the pressure drop in the case of PCMNF. Fanning friction factor of PCMNF was slightly higher than DI water at all flow rates owing to the rise in the dynamic viscosity of PCMNF over DI water. However, the enhancement in skin friction factor for

Table 3 Experimental details of present work and similar work in literature

PCM	Base fluid	Type/size of encapsulation	Melting point & latent heat	Conc.	Heat transfer test section	Reference
n-eicosane	DI water	Micro 5–15 μm	38.6 °C @ 136.2 J/g	10 wt.%	Divergent MCHS ($D_h=1.2$ mm)	[41]
n-octadecane	DI water	Micro 4.97 μm	27 °C @ 147.2 J/g	20 wt.%	Parallel MCHS ($D_h=2.71$ mm)	[22]
n-eicosane	Al ₂ O ₃ nanofluid	Micro 4–10 μm	36.3 °C (latent heat not given)	10 wt.%	Parallel MCHS ($D_h=1.2$ mm)	[49]
–	DI water	–	–	–	Rectangular microchannels ($D_h=534$ μm)	[48]
n-octadecane	PAO	Nano (size not given)	28 °C (latent heat not given)	0.3 vol.%	Microtube ($D_h=900$ μm)	[40]
n-docosane	DI water	Nano	28 °C @ 180.7 J/g	0.7 vol.%	Parallel MCHS ($D_h=2.6$ mm)	Present work

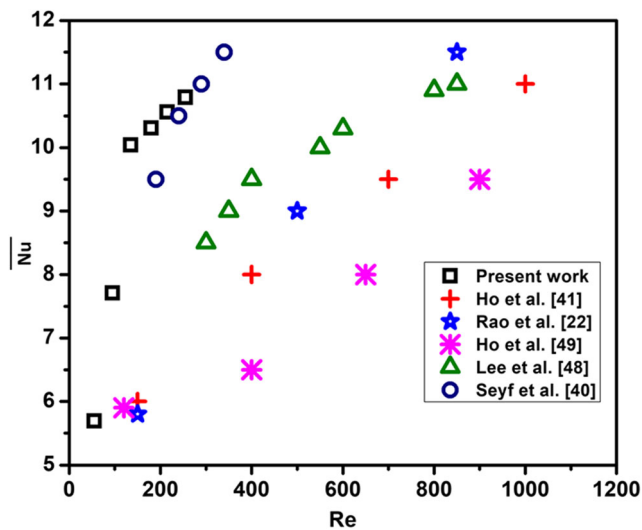


Fig. 16 Comparison of Nusselt number values between present work and previous works

PCMNF was more predominant at flow rates in the range $2.5 \times 10^{-3} \text{ kg/s}$ to $7.5 \times 10^{-3} \text{ kg/s}$, which increase the pressure drop for PCMNF corresponding to these flow rates. Due to the enhancement in friction factor for PCMNF, the pressure drop increase would be more for PCMNF than DI water.

The pumping power depends on the mass flow rate and pressure drop in the MCHS. Figure 19 shows the variation of pumping power with mass flow rate for DI water and PCMNF. The pumping power increases with mass flow rate and the trend is almost similar for PCMNF and DI water. The pumping power is directly proportional to pressure drop and since pressure drop increases with flow rate, the pumping power also increases with increase in flow rate. In comparison with DI water, the pumping power enhanced up to 23.8% for PCMNF, at the maximum flow rate in the MCHS.

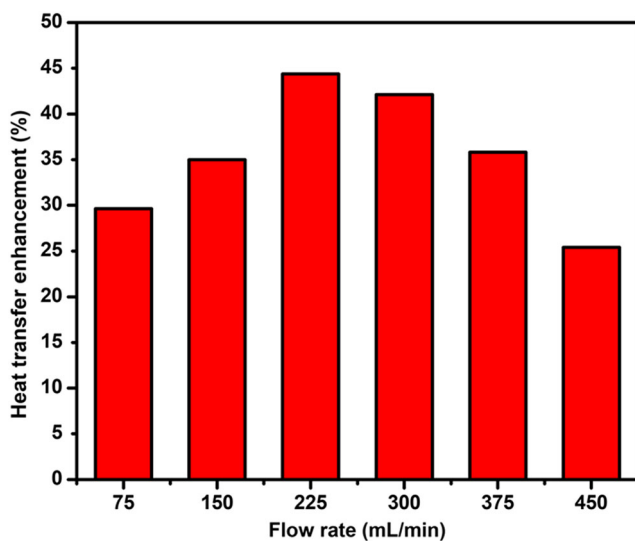


Fig. 17 Heat transfer enhancement for PCMNF over DI water with flow rates

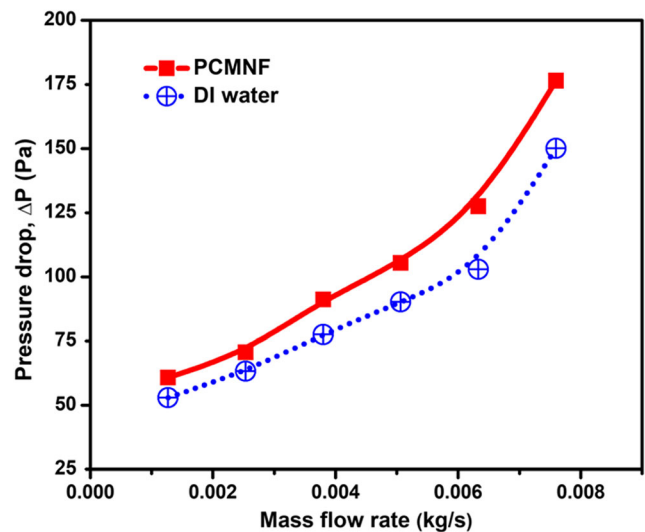


Fig. 18 Pressure drop variation with mass flow rate

5.5.8 Figure of merit

Generally, the nanofluid based heat transfer enhancement techniques in thermal systems is accompanied with the pumping power penalty. Accordingly, the effects of both heat transfer enhancement and penalty in pumping power has to be taken into account while evaluating the effectiveness of the PCMNF over DI water. FOM is based on the enhancement in average heat transfer coefficient with PCMNF over DI water against the penalty in pumping power incurred. The FOM is given by Eq. (20). If the $FOM > 1$, then the use of PCMNF is more effective compared to DI water. The variation in FOM with flow rate is given in Fig. 20. The FOM estimated for all flow rates are found to be greater than unity, which shows that PCMNF performs better than DI water. The FOM increases with flow rate, reaches a maximum and then decreases. A maximum FOM of 1.29 is obtained for PCMNF corresponding to a flow rate of 225 mL/min.

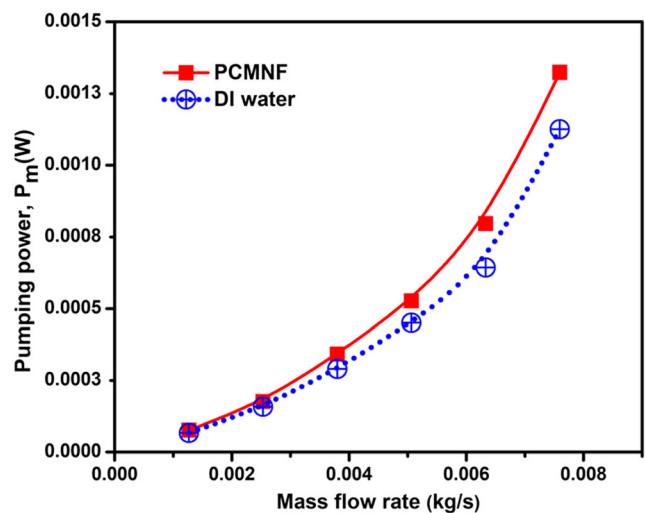


Fig. 19 Pumping power variation with mass flow rate

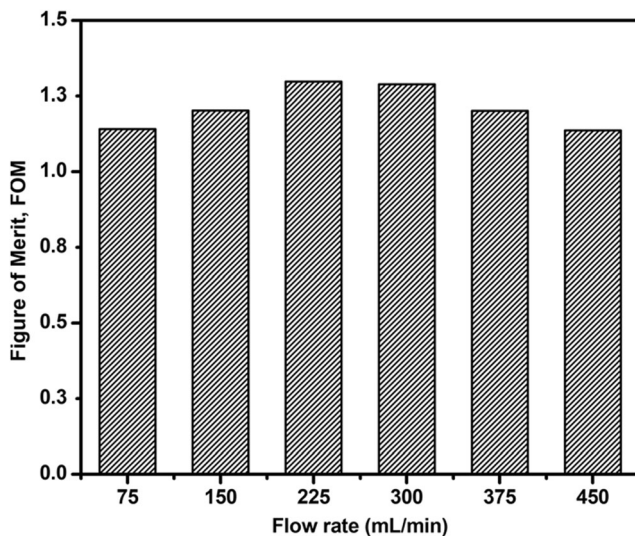


Fig. 20 Figure of merit achieved with PCMNF at different flow rates

6 Conclusion

The convective heat transfer performance of PCM based nanofluid in MCHS was studied in comparison to that of DI water. Nanoencapsulation provides excellent suspension stability and thermal stability for nanoPCM and also prevent agglomeration and leakage of PCM in the molten stage. Due to smaller particle sizes, low volume concentrations of nanoPCM is required to improve the heat capacity of base fluid. nanoPCM was synthesized by mini emulsion polymerization and dispersed in deionized water to obtain PCM nanofluid (PCMNF). While liquid cooling using minichannel heat sink is an efficient cooling method for electronics, the PCMNF provides higher average heat transfer coefficient over deionized water due to improved heat capacity owing to latent heat absorption for PCM melting. The PCMNF with 0.7% volume fraction was found to improve the heat transfer coefficient by up to 44.4% in parallel minichannel heat sink of 2.6 mm hydraulic diameter. Mass flow rate plays a crucial role in the cooling performance of PCMNF. The wall temperature and thermal resistance reduction is more distinctive when the residence time of nanoPCM in channel is more and hence the heat transfer coefficient is maximum at low flow rates. With increase in mass flow rates, the PCMNF becomes less effective and wall temperature, thermal resistance and skin friction coefficient are closer to those of deionized water, due to small residence time of PCM in the channel. For better cooling performance, the PCMNF should be operated at low mass flow rates. PCMNF is a highly stable heat transfer fluid in minichannel heat sinks and can be operated at very low flow rates with less pressure drop, pumping power and energy consumption, thus making it an ideal coolant over micro encapsulated PCM emulsions for electronics thermal management.

Availability of data and materials NA

Code availability NA

Declarations

Conflict of interest On behalf of all authors, the corresponding author states that there is no conflict of interest.

References

- Kandlikar SG, Grande WJ (2003) Evolution of microchannel flow passages—thermohydraulic performance and fabrication technology. *Heat Transfer Eng* 24(1):3–17. <https://doi.org/10.1080/01457630304040>
- Dixit T, Ghosh I (2015) Review of micro- and mini-channel heat sinks and heat exchangers for single phase fluids. *Renew Sust Energ Rev* 41:1298–1311
- Khoshvaght-Aliabadi M, Sahamiyan M (2016) Performance of nanofluid flow in corrugated minichannels heat sink (CMCHS). *Energy Convers Manag* 108:297–308. <https://doi.org/10.1016/j.enconman.2015.11.026>
- Xie XL, Liu ZJ, He YL, Tao WQ (2009) Numerical study of laminar heat transfer and pressure drop characteristics in a water-cooled minichannel heat sink. *Appl Therm Eng* 29:64–74. <https://doi.org/10.1016/j.applthermaleng.2008.02.002>
- Dang T, Teng JT (2011) Comparisons of the heat transfer and pressure drop of the microchannel and minichannel heat exchangers. *Heat Mass Transf* 47:1311–1322. <https://doi.org/10.1007/s00231-011-0793-9>
- Kebllinski P, Prasher R, Eapen J (2008) Thermal conductance of nanofluids: is the controversy over? *J Nanopart Res* 10:1089–1097. <https://doi.org/10.1007/s11051-007-9352-1>
- Colangelo G, Favale E, Milanese M, De Risi A, Laforgia D (2017) Cooling of electronic devices : Nanofluids contribution. *Appl Therm Eng* 127:421–435. <https://doi.org/10.1016/j.applthermaleng.2017.08.042>
- Roberts NA, Walker DG (2010) Convective performance of Nano fluids in commercial electronics cooling systems. *Appl Therm Eng* 30:2499–2504. <https://doi.org/10.1016/j.applthermaleng.2010.06.023>
- Murshed SMS, De Castro CAN (2017) A critical review of traditional and emerging techniques and fluids for electronics cooling. *Renew Sust Energ Rev* 78:821–833. <https://doi.org/10.1016/j.rser.2017.04.112>
- Charunyakorn P, Sengupta S, Roy SK (1990) Forced convection heat transfer in microencapsulated phase change material slurries : flow in circular ducts. *Int J Heat Mass Transf* 34:819–833
- Goel SKRM, Sengupta S (1993) The performance of liquid heat sinks with phase change material suspensions. *Int Commun Heat Mass Transf* 20:69–77
- Yamagishi Y, Takeuchi H, Pyatenko AT, Kayukawa N (1999) Characteristics of microencapsulated PCM slurry as a heat-transfer fluid. *AICHE J* 45:696–707
- Han ZH, Cao FY, Yang B (2008) Synthesis and thermal characterization of phase-changeable indium / polyalphaolefin nanofluids. *Appl Phys Lett* 92(243104):1–3. <https://doi.org/10.1063/1.2944914>
- Sarı A, Alkan C, Biçer A, Bilgin C (2014) Micro / nanoencapsulated n -nonadecane with poly (methyl methacrylate) shell for thermal energy storage. *Energy Conversion Manag* 86: 614–621. <https://doi.org/10.1016/j.enconman.2014.05.092>

15. Hong Y, Ding S, Wu W, Hu J, Voevodin AA, Gschwender L, Snyder E, Chow L, Su M (2010) Enhancing heat capacity of colloidal suspension using nanoscale encapsulated phase-change materials for heat transfer. *ACS Appl Mater Interfaces* 2:1685–1691. <https://doi.org/10.1021/am100204b>
16. Delgado M, Lázaro A, Peñalosa C, Zalba B (2014) Experimental analysis of the influence of microcapsule mass fraction on the thermal and rheological behavior of a PCM slurry. *Appl Therm Eng* 63: 11–22. <https://doi.org/10.1016/j.applthermaleng.2013.10.011>
17. Liu C, Rao Z, Zhao J, Huo Y, Li Y (2015) Review on nanoencapsulated phase change materials: preparation, characterization and heat transfer enhancement. *Nano Energy* 13:814–826. <https://doi.org/10.1016/j.nanoen.2015.02.016>
18. Doruk S, Şara ON, Karaipekli A, Yap S (2017) Heat transfer performance of water and Nanoencapsulated n -nonadecane based Nanofluids in a double pipe heat exchanger. *Heat Mass Transf* 53:1–10. <https://doi.org/10.1007/s00231-017-2072-x>
19. Jyothi NVN, Prasanna PM, Sakarkar SN, Prabha KS, Ramaiah PS, Srawan GY (2010) Microencapsulation techniques , factors influencing encapsulation efficiency. *J Microencapsul* 27:187–197. <https://doi.org/10.3109/02652040903131301>
20. Mo S, He L, Jia L, Chen Y, Cheng Z (2020) Thermophysical properties of a novel Nanoencapsulated phase change material. *Int J Thermophys* 41:1–12. <https://doi.org/10.1007/s10765-020-02641-8>
21. Salunkhe PB, Shembekar PS (2012) A review on effect of phase change material encapsulation on the thermal performance of a system. *Renew Sust Energ Rev* 16:5603–5616. <https://doi.org/10.1016/j.rser.2012.05.037>
22. Rao Y, Dammel F, Stephan P, Lin G (2007) Convective heat transfer characteristics of microencapsulated phase change material suspensions in minichannels. *Heat Mass Transf* 44:175–186. <https://doi.org/10.1007/s00231-007-0232-0>
23. Dammel F, Stephan P (2012) Heat transfer to suspensions of microencapsulated phase change material flowing through Minichannels. *J Heat Transf* 134(020907):1–8. <https://doi.org/10.1115/1.4005062>
24. Ho C, Chen W, Yan W (2013) Experimental study on cooling performance of minichannel heat sink using water-based MEPCM particles. *Int Commun Heat Mass Transf* 48:67–72. <https://doi.org/10.1016/j.icheatmasstransfer.2013.08.023>
25. Ho CJ, Chen WC, Yan WM (2014) Correlations of heat transfer effectiveness in a minichannel heat sink with water-based suspensions of Al₂O₃ nanoparticles and/or MEPCM particles. *Int J Heat Mass Transf* 69:293–299. <https://doi.org/10.1016/j.ijheatmasstransfer.2013.10.030>
26. Kong M, Alvarado JL, Terrell W, Thies C (2016) Performance characteristics of microencapsulated phase change material slurry in a helically coiled tube. *Int J Heat Mass Transf* 101:901–914. <https://doi.org/10.1016/j.ijheatmasstransfer.2016.05.047>
27. Roberts NS, Al-Shannaq R, Kurdi J, Al-Muhtaseb SA, Farid MM (2017) Efficacy of using slurry of metal-coated microencapsulated PCM for cooling in a micro-channel heat exchanger. *Appl Therm Eng* 122:11–18. <https://doi.org/10.1016/j.applthermaleng.2017.05.001>
28. Liu C, Ma Z, Wang J, Li Y, Rao Z (2017) Experimental research on flow and heat transfer characteristics of latent functional thermal fluid with microencapsulated phase change materials. *Int J Heat Mass Transf* 115:737–742. <https://doi.org/10.1016/j.ijheatmasstransfer.2017.07.107>
29. Rao JP, Geckeler KE (2011) Polymer nanoparticles : preparation techniques and size-control parameters. *Prog Polym Sci* 36:887–913. <https://doi.org/10.1016/j.progpolymsci.2011.01.001>
30. Fuensanta M, Paiphansiri U, Romero-Sánchez MD, Guillem C, López-Buendía ÁM, Landfester K (2013) Thermal properties of a novel nanoencapsulated phase change material for thermal energy storage. *Thermochim Acta* 565:95–101. <https://doi.org/10.1016/j.tca.2013.04.028>
31. Zhang GH, Bon SAF, Zhao CY (2012) Synthesis , characterization and thermal properties of novel nanoencapsulated phase change materials for thermal energy storage. *Sol Energy* 86:1149–1154. <https://doi.org/10.1016/j.solener.2012.01.003>
32. Fang Y, Yu H, Wan W, Gao X, Zhang Z (2013) Preparation and thermal performance of polystyrene / n-tetradecane composite nanoencapsulated cold energy storage phase change materials. *Energy Convers Manag* 76:430–436. <https://doi.org/10.1016/j.enconman.2013.07.060>
33. Fang Y, Kuang S, Gao X, Zhang Z (2009) Preparation of nanoencapsulated phase change material as latent functionally. *J Phys D Appl Phys* 42(035407):1–8. <https://doi.org/10.1088/0022-3727/42/3/035407>
34. Chen Z, Yu F, Zeng X, Zhang Z (2012) Preparation , characterization and thermal properties of nanocapsules containing phase change material n -dodecanol by miniemulsion polymerization with polymerizable emulsifier. *Appl Energy* 91:7–12. <https://doi.org/10.1016/j.apenergy.2011.08.041>
35. Fang Y, Liu X, Liang X, Liu H, Gao X, Zhang Z (2014) Ultrasonic synthesis and characterization of polystyrene / n-dotriacontane composite nanoencapsulated phase change material for thermal energy storage. *Appl Energy* 132:551–556. <https://doi.org/10.1016/j.apenergy.2014.06.056>
36. De Castro PF, Shchukin DG (2015) New polyurethane / Docosane microcapsules as phase-change materials for thermal energy storage. *Chem Eur J* 21:11174–11179. <https://doi.org/10.1002/chem.201500666>
37. Shchukina EM, Graham M, Zheng Z, Shchukin DG (2018) Nanoencapsulation of phase change materials for advanced thermal energy storage systems. *Chem Soc Rev* 47:4156–4175. <https://doi.org/10.1039/C8CS00099A>
38. Wu W, Bostanci H, Chow LC, Ding SJ, Hong Y, Su M, Kizito JP, Gschwender L, Snyder CE (2011) Jet impingement and spray cooling using slurry of nanoencapsulated phase change materials. *Int J Heat Mass Transf* 54:2715–2723. <https://doi.org/10.1016/j.ijheatmasstransfer.2011.03.022>
39. Wu W, Bostanci H, Chow LC, Hong Y, Wang CM, Su M, Kizito JP (2013) Heat transfer enhancement of PAO in microchannel heat exchanger using nano-encapsulated phase change indium particles. *Int J Heat Mass Transf* 58:348–355. <https://doi.org/10.1016/j.ijheatmasstransfer.2012.11.032>
40. Seyf HR, Zhou Z, Ma HB, Zhang Y (2013) Three dimensional numerical study of heat-transfer enhancement by nano-encapsulated phase change material slurry in microtube heat sinks with tangential impingement. *Int J Heat Mass Transf* 56:561–573. <https://doi.org/10.1016/j.ijheatmasstransfer.2012.08.052>
41. C.J. Ho, S. Hsu, S. Rashidi, W. Yan (2020) Water-based nano-PCM emulsion flow and heat transfer in divergent mini-channel heat sink — an experimental investigation. *Int J Heat Mass Transf* 146: 118861 1–11. doi:<https://doi.org/10.1016/j.ijheatmasstransfer.2019.119086>
42. Joseph M, Sajith V (2019) An investigation on heat transfer performance of polystyrene encapsulated n-octadecane based nano fluid in square channel. *Appl Therm Eng* 147:756–769. <https://doi.org/10.1016/j.applthermaleng.2018.10.120>
43. Kuravi S, Du J, Chow LC (2010) Encapsulated phase change material slurry flow in manifold microchannels. *J Thermophys Heat Transf* 24:364–373. <https://doi.org/10.2514/1.44276>
44. Rajabifar B (2015) Enhancement of the performance of a double layered microchannel heatsink using PCM slurry and nanofluid coolants. *Int J Heat Mass Transf* 88:627–635. <https://doi.org/10.1016/j.ijheatmasstransfer.2015.05.007>
45. Taylor JR (1997) Introduction to error analysis 2ed.pdf

46. Vallar S, Houivet D, El Fallah J, Kervadec D, Haussonne J (1999) Oxide slurries stability and powders dispersion : optimization with zeta potential and rheological measurements. *J Eur Ceram Soc* 19: 1017–1021
47. Kandlikar SG, Garimella S, Li D, Colin S, King MR (2006) *Heat Transfer and Fluid Flow in Minichannels and Microchannels*, 1st edn 2006 Elsevier Ltd. ISBN: 0-0804-4527-6
48. Lee PS, Garimella SV, Liu D (2005) Investigation of heat transfer in rectangular microchannels. *Int J Heat Mass Transf* 48:1688–1704
49. Ho CJ, Chen WC (2013) An experimental study on thermal performance of Al₂O₃/water nanofluid in a minichannel heat sink. *Appl Therm Eng* 50:516–522

Publisher's note Springer Nature remains neutral with regard to jurisdictional claims in published maps and institutional affiliations.